Functionally Distinct Connectivity of Developmentally Targeted Striosome Neurons

Matthew M. McGregor[1,2,3,6], **Gabriel L. McKinsey**[1,2,5,6], **Allison E. Girasole**[1,2,3], **Chloe J. Bair-Marshall**[4], **John L.R. Rubenstein**[2,3,5,7], **Alexandra B. Nelson**[1,2,3,4,7,8,*]

[1]Neuroscience Graduate Program, UCSF, San Francisco, CA 94158, USA

[2]Weill Institute for Neurosciences, UCSF, San Francisco, CA 94158, USA

[3]Kavli Institute for Fundamental Neuroscience, UCSF, San Francisco, CA 94158, USA

[4]Department of Neurology, UCSF, San Francisco, CA 94158, USA

[5]Department of Psychiatry, UCSF, San Francisco, CA, 94158, USA

[6]These authors contributed equally

[7]Senior author

[8]Lead Contact

SUMMARY

One long-standing model of striatal function divides the striatum into compartments called striosome and matrix. While some anatomical evidence suggests that these populations represent distinct striatal pathways with differing inputs and outputs, functional investigation has been limited by the methods for identifying and manipulating these populations. Here, we utilize *hs599*^{CreER} mice as a new tool for targeting striosome projection neurons and testing their functional connectivity. Extending anatomical work, we demonstrate that striosome neurons receive greater synaptic input from prelimbic cortex, whereas matrix neurons receive greater input from primary motor cortex. We also identify functional differences in how striosome and matrix neurons process excitatory input, providing the first electrophysiological method for delineating striatal output neuron subtypes. Lastly, we provide the first functional demonstration that striosome neurons are the predominant striatal output to substantia nigra pars compacta dopamine neurons. These results identify striosome and matrix as functionally distinct striatal pathways.

*Correspondence: alexandra.nelson@ucsf.edu.

Graphical Abstract

In Brief

McGregor et al. utilize a novel transgenic mouse line to dissect the functional circuitry and electrophysiology of striatal striosome and matrix neurons. They report that striosome and matrix neurons receive distinct synaptic input and that striosome neurons represent the major striatal population innervating substantia nigra pars compacta dopamine neurons.

INTRODUCTION

The striatum is the primary input nucleus of the basal ganglia and plays a critical role in a wide range of behaviors. Classical models of striatal function divide the output neurons, medium spiny neurons (MSNs), into two groups: direct and indirect pathway cells. These populations have proven useful for understanding striatal functions such as movement control (Kravitz and Kreitzer, 2012; Cui et al., 2013) and are differentiated by their connectivity to downstream basal ganglia nuclei. An alternative model that may help explain other striatal functions, including certain forms of learning and decision making (Brown et al., 1999; Friedman et al., 2015), divides striatal output neurons into populations called striosome and matrix. Like the direct-indirect pathway model, striosome and matrix neurons are hypothesized to mediate distinct functions, based in large part on proposed differences in their upstream and downstream connectivity.

Historically, striosome and matrix neurons have been distinguished by their localization within neurochemically distinct compartments. Striosome compartments, which appear as irregularly distributed islands within the surrounding matrix, show enriched expression of markers such as μ-opioid receptors (MORs) and diminished expression of markers such as calbindin (Pert et al., 1976; Gerfen, 1985). Early and recent anatomical tracing studies found that terminals from limbic and sensorimotor regions show preferential localization in striosome and matrix compartments, respectively (Ragsdale and Graybiel, 1988; Sadikot et al., 1992; Eblen and Graybiel, 1995; Kincaid and Wilson, 1996; Lévesque and Parent, 1998; Friedman et al., 2015). Additionally, while MSNs in both compartments project to canonical downstream basal ganglia targets such as the substantia nigra pars reticulata (SNr), tracing studies suggest that striosome MSNs in the dorsal striatum send additional output to dopamine neurons in the substantia nigra pars compacta (SNc), while those in the ventral striatum project to dopamine neurons in the ventral tegmental area (VTA) (Gerfen, 1985; Jiménez-Castellanos and Graybiel, 1989; Fujiyama et al., 2011; Watabe-Uchida et al., 2012). These anatomical findings led to the hypothesis that striosomes comprise a distinct striatal pathway that integrates limbic information and regulates activity of SNc dopamine neurons.

Neurochemically defined striosome and matrix compartments have been recognized for decades, but without tools to identify and manipulate these neurons *in vivo*, studies of how potential structural differences in connectivity translate functionally have been limited. Much of our current knowledge is derived from post-mortem neuroanatomical studies, with methods to facilitate functional study of striosome and matrix MSNs in living tissue only recently becoming available (Davis and Puhl, 2011; Gerfen et al., 2013; Banghart et al., 2015; Lopez-Huerta et al., 2016; Smith et al., 2016; Crittenden et al., 2017). Such approaches have enabled novel insights into differences between striosome and matrix but also raised debate over whether striosome and matrix MSNs indeed differ in their inputs and outputs. Here, we use Cre-mediated recombination from the hs599[CreER] mouse line to target developing striosome MSNs. We find that striosome and matrix MSNs receive biased input from limbic and sensorimotor regions at the synaptic level. We also show that striosome and matrix MSNs have divergent intrinsic properties. Finally, we demonstrate that striosome and matrix MSNs have functionally distinct inhibitory output to SNc dopamine neurons. Together, our data establish the *hs599*[CreER] mouse line as a highly specific tool for studying striosomes and confirm that striosome and matrix represent functionally distinct striatal pathways.

RESULTS

Enhancer hs599 Drives Gene Expression in Postmitotic Neurons of the Developing Striatum

hs599 is a 1,678-bp DNA fragment from the human genome that was discovered to drive *LacZ* expression in the embryonic day 11.5 (E11.5) mouse striatum using a mouse transgenic screen of candidate regulatory elements (Visel et al., 2013). hs599 was then cloned upstream of *CreERT2-IRES-eGFP* and used to generate a stable mouse transgenic line (*hs599*[CreERT2-EGFP], referred to here as *hs599*[CreER]), which confirmed its activity in the

E11.5 striatum (Silberberg et al., 2016). Here, we investigated *hs599*^{CreER} as a tool for labeling components of the developing striatum.

To explore its ability to label striosomes, we examined hs599-driven CreER-eGFP expression and CreER-mediated recombination during development following a single administration of tamoxifen. Previous studies demonstrate that striosome and matrix cells are derived from the lateral ganglionic eminence (LGE) starting at E10.5 (van der Kooy and Fishell, 1987), with striosome neurons born prior to matrix neurons. Because the hs599 is active in the LGE during this time (Silberberg et al., 2016), we hypothesized that tamoxifen administration at E10.5 would label early-born neurons that give rise to striosomes (Figure 1A). Therefore, we administered tamoxifen at E10.5 to *hs599*^{CreER};Ai14 mice and observed CreER-eGFP expression (EGFP) and Cre-mediated recombination (tdTomato) in the striatum of embryos and pups (E12.5, E15.5, and E18.5; Figures 1B and S1A-S1C). In the LGE at E12.5, recombination appeared restricted to the neuronal zone (mantle zone), suggesting hs599 was not active in progenitor cells (Figure 1B). To confirm that recombination was restricted to post-mitotic cells, we stained E12.5 sections for either Ki67 or phospho-histone H3, markers of proliferating cells. Neither eGFP nor Cre-driven tdTomato expression overlapped with either marker within the LGE, except for a small domain at the pallial/subpallial boundary (Figures 1C and 1D, asterisks in Figure S1A). This region produces interneurons of the olfactory bulb and pyramidal neurons of the piriform cortex; both of these structures had low levels of recombination (Figure 1E). No recombination was observed in the progenitor domains of the medial ganglionic eminence (Figure 1B). While we did observe recombined cells in the external globus pallidus (GPe), they were NKX2-1 negative and therefore unlikely to be derived from the MGE (Figure S2A) (Flandin et al., 2010; Nóbrega-Pereiraetal., 2010; Hernández etal., 2015; Dodson et al., 2015). In line with hs599 enhancer embryonic activity, fate mapping of tdTomato^{+} cells in adult animals (postnatal day 30 [P30]) revealed labeling in the GABAergic regions of the telencephalon (striatum, olfactory bulb, olfactory tubercle, septal nuclei, bed nucleus of the stria terminalis [BNST], amygdala [central and intercalated nucleus], and diencephalon [reticular thalamus and zona incerta]) (Figure 1E). Notably, tdTomato[+] cell bodies were not observed in the substantia nigra (Figures 1E and S2B). These data show that *hs599*^{CrsER} mice can be used to label a subset of striatal neurons born during specific developmental time points.

hs599^{CreER} Mice Enable Genetic Targeting of Striosome MSNs

hs599^{CreER};Ai14 mice given tamoxifen at E10.5 lead to patchy striatal tdTomato expression by adulthood, suggesting the possibility of striosome labeling (Figure 1B, right). To test this hypothesis, we double-labeled striatal sections from *hs599*^{CreER};Ai14 mice for MORs and calbindin, markers of striosome and matrix compartments, respectively (Pert et al., 1976; Gerfen et al., 1985). tdTomato^{+} cells were found in regions enriched for MOR and poor in calbindin expression (Figures 2A and 2B), consistent with striosome labeling. Previous studies targeting striosomes developmentally indicate a tradeoff between penetrance and specificity across different developmental time points (Kelly et al., 2018; van der Kooy and Fishell, 1987; Mason et al., 2005). Therefore, we estimated the penetrance and specificity of striosome labeling in the dorsal striatum of *hs599*^{CrsER};Ai14 mice (tamoxifen administration

at E10.5) by quantifying the density of tdTomato$^+$ cells in striosome and matrix compartments (Figures 2C and 2D). We observed an ~12-fold higher density of labeling in striosome compared to matrix compartments ($12,211 \pm 820$ versus $1,058 \pm 79$ cells/mm, N = 3; Figure 2I). Notably, tamoxifen administration at E15.5 led to increased striatal labeling, but in a broader and more nonspecific pattern (data not shown). Next, to confirm whether labeling was restricted to striatal projection neurons (MSNs), we stained for markers of striatal interneurons: choline acetyltransferase (ChAT), parvalbumin (PV), and neuropeptide Y (NPY) (Figures 2E-2G). We observed almost no overlap of tdTomato with ChAT, PV, or NPY (Figure 2J). These findings indicate that *hs599*^{CreER} mice enable highly enriched labeling of striosome MSNs.

Striosome and matrix compartments each contain direct and indirect pathway MSNs. To determine if *hs599*^{CreER} mice preferentially label either pathway, we first measured the endogenous proportion of indirect pathway MSNs in each compartment. Striatal slices from an indirect pathway reporter mouse line (D2-GFP; Gong et al., 2003) were stained for MORs and the neuronal marker NeuN, enabling quantification of the proportion of GFP$^+$ neurons in striosomes and matrix (Figure 2H). While approximately half of identified matrix neurons were GFP$^+$ ($45.8\% \pm 0.6\%$, N = 4), striosomes showed a small but consistent reduction in this proportion ($38.7\% \pm 1.2\%$, N = 4), suggesting a slight enrichment for direct pathway MSNs (Figure 2K). Using *hs599*^{CreER};Ai14;D2-GFP mice, we next quantified the proportion of tdTomato$^+$ neurons that were D2-GFP$^+$. We observed minimal overlap between GFP$^+$ and tdTomato$^+$ neurons (Figures 2H and 2K; $9.8\% \pm 0.9\%$, N = 3), indicating that labeled neurons in *hs599*^{CreER} mice underrepresent indirect pathway MSNs within striosomes. Thus, our data indicate that striatal neurons labeled in *hs599*^{CreER} mice are primarily direct pathway striosome MSNs.

Striosome and Matrix Receive Differential Input from Prelimbic and Primary Motor Cortex

The advent of novel tools for studying striosome and matrix MSNs has raised questions over whether these populations receive differing levels of input from limbic and sensorimotor neocortical regions. With the *hs599*^{CreER} mouse line as a tool to identify and manipulate striosome MSNs, we next tested the hypothesis that striosome MSNs receive differential inputs from upstream brain regions, as compared to neighboring matrix MSNs. While terminals from prelimbic cortex (PL) and primary motor cortex (M1) have been found to preferentially distribute onto striosome and matrix compartments, respectively (Eblen and Graybiel, 1995; Kincaid and Wilson, 1996; Lévesque and Parent, 1998; Miyamoto et al., 2018), it is unknown how such anatomical differences translate at the functional level. To address this question, we expressed channelrhodopsin (ChR2-EYFP) in either the PL or M1 of *hs599*^{CreER};Ai14 mice. Consistent with previous findings, ChR2-EYFP$^+$ fibers from the PL were enriched in tdTomato-labeled striosomes (Figures S3A-S3C), while those from M1 concentrated in the matrix (Figures S3D-S3F). Next, we targeted sequential pairs of neighboring striosome and matrix MSNs in *ex vivo* brain slices (Figure 3A) and measured optically evoked excitatory postsynaptic currents (oEPSCs) in whole-cell voltage-clamp configuration. Brief pulses of blue light induced short-latency oEPSCs (<5 ms) from PL and M1 inputs in both matrix and striosome MSNs (Figure 3A). The amplitude of PL-derived EPSCs was greater in striosome (776 ± 175 pA) than in matrix (483 ± 182 pA) MSNs

(Figure 3B, left; Wilcoxon sign-rank, p = 0.0099, n = 17 pairs, N = 4). Conversely, the amplitude of M1-derived EPSCs was significantly lower in striosome (202 ± 48 pA) compared to matrix (756 ± 201 pA) MSNs (Figure 3C, left; Wilcoxon sign-rank, p = 0.0072, n = 19 pairs, N = 4). To quantify the functional bias of PL and M1 inputs for striosome MSNs, we averaged the ratio of oEPSC amplitudes [striosome/(striosome + matrix)] for all recorded pairs, as well as for each animal. Values greater than 0.5 represent preference for striosome MSNs, while values less than 0.5 represent preference for matrix MSNs. The PL and M1 showed opposing biases, with the PL favoring striosome MSNs (Figure 3B, right; 0.65) and the M1 favoring matrix MSNs (Figure 3C, right; 0.28). The directionality of this bias was consistent across all animals for both the PL and M1. In combination, these results extend anatomical findings, showing that PL and M1 inputs onto individual striosome and matrix MSNs differ at the functional level.

Direct Pathway Striosome MSNs Have Increased Intrinsic Excitability Compared to Matrix MSNs

Though striosome and matrix MSNs may receive distinct synaptic input from the PL and M1, how they transform synaptic input into spiking relies in part on their intrinsic properties. Using whole-cell current-clamp recordings in *ex vivo* brain slices to measure instantaneous firing rates in response to current injections, we compared the intrinsic excitability of striosome and matrix MSNs (Figures 3D and 3E). To control for potential differences in excitability between direct and indirect pathway MSNs (Gertler et al., 2008; Lieberman et al., 2018; Planert et al., 2013), we used *hs599*^{CreER};Ai14;D2-GFP mice to compare labeled striosome MSNs to direct and indirect pathway MSNs in the matrix. As very few labeled striosome neurons were indirect pathway neurons (Figure 2K), only direct pathway MSNs within striosomes were examined (see STAR Methods). Because direct pathway MSNs have lower intrinsic excitability than indirect pathway MSNs, we would expect to see lower excitability in tdTomato$^+$ striosome MSNs than matrix MSNs. However, we observed higher intrinsic excitability in labeled striosome MSNs (n = 34, N = 5) than matrix MSNs (Figure 3F; n = 25, N = 5). In fact, intrinsic excitability of presumed direct pathway striosome MSNs (n = 34, N = 5) was increased over both direct (Figure 3G; n = 12, N = 5) and indirect (Figure 3H; n = 13, N = 5) pathway MSNs in the matrix. Histologically confirmed direct pathway striosome MSNs showed similar excitability to that of the overall striosome population (Figure S3G). No difference was observed in the maximal firing rate (Figure S3H; striosome = 50 ± 3.0 spikes/s, matrix D1 = 55 ± 4.4 spikes/s, matrix D2 = 51 ± 5.4 spikes/s; Kruskal-Wallis, p = 0.595) or resting membrane potential (Figure S3I; striosome = −89 ± 0.9 mV, matrix D1 = −93 ± 1.5 mV, matrix D2 = −87 ± 1.4 mV; Kruskal-Wallis, p = 0.032) of any group. However, direct pathway striosome MSNs had higher input resistance at rest (Figure S3J; striosome = 236 ± 14 MΩ, matrix D1 =151 ± 16 MΩ, matrix D2 = 162 ± 25 MΩ; Kruskal-Wallis, p = 0.00052, Dunn post hoc, striosome versus D1 matrix, p = 0.0018, D2 matrix, p = 0.0023) and showed a substantial shift in rheobase (Figure S3K; striosome = 207 ± 17 pA, matrix D1 = 404 ± 47 pA, matrix D2 = 325 ± 32 pA; Kruskal-Wallis, p < 0.0001, Dunn post hoc, striosome versus D1 matrix p < 0.0001, D2 matrix p = 0.0008). Given the marked difference in excitability between striosome and matrix MSNs, we wondered if this electrophysiological property could be used as a surrogate marker for compartmental identity. Striosome and matrix direct pathway MSNs showed minimal

overlap in their rheobase distribution (Figure S3K). Therefore, we quantified the positive and negative predictive value (PPV and NPV) of various rheobase cutoffs for identifying direct pathway MSNs in striosomes from those in the matrix (Figures S3L-S3N). Notably, a rheobase cutoff of 200 pA or less had a PPV of 100% for labeled striosome neurons, while a rheobase cutoff of 250 pA or more had a NPV of 92.7% (Figures S3L and S3M). Repeating this measure without *a priori* knowledge of direct or indirect pathway identity produced similar results (Figure S3N; PPV = 76.9%, NPV = 92.0%) Together, these data indicate striosome MSNs have greater intrinsic excitability than matrix MSNs of either pathway and provide a potential non-transgenic approach for electrophysiological identification of direct pathway striosome MSNs in slice recordings.

Striosome MSNs Are a Predominant Source of Striatal Input to SNc Dopamine

We next asked if striosome MSNs send outputs to distinct downstream targets. Previous anatomical studies suggest that direct pathway striosome MSNs, unlike those in the matrix, project monosynaptically to substantia nigra pars compacta (SNc) dopamine neurons, in addition to canonical target regions such as the substantia nigra pars reticulata (SNr) (Gerfen, 1985; Jiménez-Castellanos and Graybiel, 1989; Fujiyama et al., 2011; Watabe-Uchida et al., 2012; Yang et al., 2018). However, this anatomical connection from striosome MSNs to SNc dopamine neurons and its specificity have not been explored at the physiological level. Furthermore, recent evidence suggested that striosome output may not differ from that of matrix (Smith et al., 2016). To address if striosome MSN synaptic output is distinct from that of direct pathway MSNs as a whole, we expressed ChR2-eYFP in direct pathway MSNs (both striosome and matrix; D1-Cre;Ai32) or selectively within striosome MSNs ($hs599^{CreER}$;Ai32) and recorded light-evoked currents in SNc dopamine neurons. To control for differences in ChR2 expression across lines, we also recorded light-evoked currents in SNr neurons, allowing for normalization of synaptic output as a ratio between the two target regions (SNc/SNr; Figure 4A). In both D1-Cre;Ai32 (D1) and $hs599^{CreER}$;Ai32 (599) mice, we observed ChR2-EYFP$^+$ terminals within the SNc as identified by staining for tyrosine hydroxylase, a marker of dopaminergic neurons (Figures S4A and S4B). Brief pulses of blue light induced optically evoked inhibitory postsynaptic currents (oIPSCs) with short latency (<5 ms), which were unaffected by application of glutamatergic antagonists (2,3-dihydroxy-6-nitro-7-sulfamoylbenzo[f]quinoxaline [NBQX] + [2*R*]-amino-5-phosphonovaleric acid [APV]) and abolished by application of the GABA$_A$ antagonist picrotoxin (Figures 4B and 4C). In SNc dopamine neurons identified by biocytin fill (Figure S4C) or cell-attached spike waveform (Figures S4D and S4E), we observed no difference in the oIPSC amplitude between 599 and D1 mice (Figure 4D; 599 = 428 ± 145 pA, n = 9, N = 5; D1 = 281 ± 109 pA, n = 7, N = 5; p = 0.70). If we assume that D1-Cre captures all direct pathway neurons, these results indicate that the majority of striatal input to SNc dopamine neurons is derived from striosome neurons. Consistent with this assumption, oIPSC amplitude in SNr neurons was significantly less in 599 compared to D1 mice (Figure 4E; 599 = 1,603 ± 505 pA, n = 14, N = 5; D1 = 4,417 ± 392 pA, n = 14, N = 5; p = 0.0012). The normalized ratio oIPSC amplitude (SNc:SNr) averaged 0.25 in 599 mice and 0.06 in D1 mice, suggesting that striosome output shows increased bias toward SNc dopamine neurons compared to D1 MSNs as a whole. To compare these ratios statistically, we bootstrapped data acquired from D1 and 599 mice to obtain a probability distribution of outcomes, which

were significantly different (Figure 4F; Kolmogorov-Smirnov test, p < 0.001). Next, to show that striosome MSNs can regulate SNc dopamine neuron firing, we recorded spontaneous activity of dopamine neurons in a cell-attached configuration and activated striosome terminals using $hs599^{CreER}$;Ai32 mice and brief trains of blue light (5 pulses, 10 Hz; Figure 4G). Activation of striosome MSNs was sufficient to inhibit firing in SNc dopamine neurons (Figure 4H; n = 7, N = 4). Thus, these results demonstrate that striosome MSNs are the major source of striatal output to SNc dopamine neurons.

DISCUSSION

As a new tool for studying striosome and matrix MSNs, it is important to consider how the $hs599^{CreER}$ mouse line compares to existing methods. Our data indicate that by targeting early-born, postmitotic neurons of the LGE, $hs599^{CreER}$ mice label striosomes with higher specificity compared to non-inducible Cre lines, such as the Sepw1NP67-Cre line (Smith et al., 2016), though with reduced penetrance. Labeling of more ventral striosomes was especially variable, being present in some mice but appearing largely absent in others. As with other mouse lines for targeting striosomes (Kelly et al., 2018; Smith et al., 2016), labeling in $hs599^{CreER}$ mice was present in MSNs, but not major interneuron populations. Furthermore, labeling within MSNs was strongly biased toward those of the direct pathway, a feature of other methods for targeting striosomes (Davis and Puhl, 2011; Banghart et al., 2015; Smith et al., 2016). Although our data support a slightly greater proportion of direct pathway MSNs in striosomes compared to matrix, labeling with these lines and $hs599^{CreER}$ mice underrepresents the numbers of indirect pathway MSNs in striosomes. The presence of this bias across different methods for isolating striosomes may suggest that molecular differences between striosome and matrix are more marked across direct pathway than indirect pathway MSNs. It is important to note though that other developmental strategies have produced more even labeling of indirect and direct pathway MSNs in striosomes, suggesting that the bias observed in $hs599^{CreER}$ mice results from regulation of CreER expression, rather than developmental timing (Kelly et al., 2018). Thus, $hs599^{CreER}$ mice may be particularly useful when high specificity of striosome labeling is required, or for studying dorsal direct pathway striosome MSNs in particular.

Using the $hs599^{CreER}$ mouse line, we found that at the functional level, PL inputs preferentially target striosome MSNs, whereas M1 inputs preferentially target matrix MSNs. These results are consistent with previous anterograde tracing studies using traditional neurochemically defined striosomes. However, it is important to integrate these local differences in innervation across striosome and matrix with the differences present across anatomical axes, such as dorsoventral and mediolateral. Inputs to striosome and matrix are highly heterogeneous across these axes, meaning that inputs to MSNs in neighboring compartments may be more similar than when compared to distant MSNs in the corresponding compartment. It is likely then that, like matrix MSNs, striosome MSNs in different striatal regions serve distinct functions. Recent work has highlighted the molecular heterogeneity of striosomes throughout the striatum (Miyamoto et al., 2018); future studies should aim to extend such analysis to the level of *in vivo* activity and behavior.

We also found higher intrinsic excitability in direct pathway striosome MSNs compared to those in the matrix, which may amplify differences in excitatory inputs. In fact, the nearly nonoverlapping rheobases of striosome and matrix MSNs may provide a new means of studying striosome MSNs in slice preparations, without transgenic labeling. However, additional validation across genetic backgrounds and ages will be necessary. Critically important is how these differences in both excitatory inputs and intrinsic properties affect activity patterns *in vivo*. Calcium imaging in awake mice indicates that reward-predictive stimuli elicit stronger responses in striosomes than in matrix (Bloem et al., 2017; Yoshizawa et al., 2018). This difference might be explained by differences in intrinsic excitability, though contributions from glutamatergic and dopaminergic input remain to be examined.

Lastly, we provide evidence that striosome MSNs account for the majority of striatal inhibitory input onto SNc dopamine neurons. With the differences in cortical inputs described here, and the segregation of lateral connectivity between striosome and matrix populations shown previously (Kawaguchi et al., 1989; Banghart et al., 2015), these data support the long-standing hypothesis that striosome and matrix neurons constitute functionally distinct striatal pathways. However, how the activity of striosome neurons, or their inhibition of dopamine neurons, shapes behavior remains an open question. Recent calcium-imaging studies indicate that genetically defined striosome and matrix MSNs are activated by reward (Bloem et al., 2017; Yoshizawa et al., 2018), but striosome output to SNc dopamine neurons suggests that the response of striosome neurons may have distinct effects compared to matrix MSNs. This hypothesis is supported by recent studies showing that manipulations targeting striosome or matrix-biased cortical inputs bias decision-making in different ways (Friedman et al., 2015, 2017). Based on basal ganglia actor-critic models, striosome input may suppress reward-driven responses when rewards are expected (Brown et al., 1999).

Our finding that striosome activation is sufficient to alter spontaneous firing of SNc dopamine neurons suggests that striosome MSNs could fill such a role. Understanding how striosome inputs shape dopamine neuron activity in vivo may clarify the true functional role of striosome MSNs. Together, our results reestablish the striosome and matrix as functionally distinct striatal pathways and provide a new tool for investigating the role of striosomes in behavior.

STAR★METHODS

LEAD CONTACT AND MATERIALS AVAILABILITY

Additional information and requests for resources and reagents should be directed to and will be fulfilled by the Lead Contact, Alexandra Nelson (Alexandra.Nelson@ucsf.edu). This study did not generate new unique reagents.

EXPERIMENTAL MODEL AND SUBJECT DETAILS

Animals—Prenatal and adult mice of either sex (age >6 weeks) from six different transgenic lines were used in this study. For histological experiments and identification of striosomes in slice, hemizygous *hs599^{CrsER}* females (CD-1 IGS, Silberberg et al., 2016)

were crossed to homozygous Ai14 (C57BL/6, Madisen et al., 2010) male breeders, to yield experimental animals hemizygous for both Ai14 and *hs599*^{CreER}. To identify indirect and direct pathway neurons within striosome and matrix compartments, homozygous Ai14 (C57BL/6) and hemizygous D2-GFP mice (C57BL/6; Gong et al., 2003) were crossed, with male hemizygous offspring subsequently bred to *hs599*^{CreER} (CD1) females. Experimental animals from this cross were hemizygous for D2-GFP, Ai14, and *hs599*^{CreER}. Finally, expression of ChR2-eYFP in striosome or direct pathway neurons was produced by crossing homozygous Ai32 (C57/BL6, Madisen et al., 2012) males to either hemizygous *hs599*^{CreER} or D1-Cre (C57BL/6, Gerfen et al., 2013) females, respectively, yielding mice hemizygous for Ai32 and D1-Cre or *hs599*^{CreER}. All animals were housed 1-5 per cage and maintained on 12 hr light/dark cycle with food and water provided *ad libitum.* Experimental procedures were carried out with approval of the Institutional Animal Care and Use Committee at University of California, San Francisco and complied with local and national ethical and legal regulations regarding research using mice.

METHOD DETAILS

Genotyping of hs599^{CreER} mice—For *hs599*^{CreER} mice, tail biopsies were digested overnight at 55°C in 200 μL of buffer containing 50 mM KCl, 10 mM Tris-HCl (pH 8.3), 2.5 mM MgCl2-6H2O, 0.1 mg/mL gelatin, 0.45% IGEPAL CA-630 (by volume), 0.45% Tween 20 (by volume), and 0.25 mg/mL proteinase K. Tails were then boiled for 10 min and spun down for 5 min at 2400 rpms. Next, supernatant (1 μL) was added to a mixture of dNTPs (2.5 μL), 10X LA PCR Buffer II (Mg^{2+} plus) (2.5 μL), dH20 (17.75 μL), forward primer (1 μL, CACTACTGTTTCTAAGTGTTTCC), and reverse primer (1 μL, CAGCACAGGCTCAAAGTTGCC). PCR conditions were as follows: 93°C for 3 min, then hold at 82°C and 0.25 μL TaKaRa LA Taq added. Then, 35 cycles of 93°C for 30 s, 58°C for 30 s, 65°C for 30 s. Products were held at 4°C, then run on a 1% agarose gel with SYBR Safe for 40 min at 110 V. Gels were imaged with UV light and presence of the transgene was indicated by a 398bp band.

Tamoxifen Administration—Activation of transgene expression in striosome neurons was achieved by orally gavaging female hs599^{CreER} breeders with tamoxifen (125 mg/kg) dissolved in corn oil (20 mg/mL) on developmental day E10.5. Developmental time points were determined by checking mice each morning for vaginal plugs, with 12:00 pm set as E0.5 following plug detection.

Virus Injections—Anesthesia was induced with intraperitoneal injection of ketamine-xylazine (15-30 mg), after which mice were placed in a stereotaxic frame (Kopf Instruments). Anesthesia was maintained with 1% isoflurane (inhaled) for the duration of the procedure. After opening the scalp, a mounted drill was used to make bilateral burr holes above either prelimbic (PL) or primary motor (M1) cortex. Next, 250 μL of AAV5-hSyn-hChR2(H134R)-eYFP (UNC Vector Core) was delivered using a 33 gauge blunt needle and Micro4 pump (WPI) at 50 nL/min at the following coordinates relative to bregma and surface of the dura (in mm): PL, AP: +2.5 ML: ± 0.3 DV −1.0; M1, AP: +1.2 ML: ± 1.6 DV: −0.8. Ten minutes after completion of the injection, the needle was removed, the scalp sutured, and animals kept on a heating pad until awakening. Virus was allowed to express for

a minimum of 6 weeks prior to experimentation. Injection sites were confirmed following recordings using a Nikon 6D conventional wide-field microscope. Notably, in one animal injected with virus in M1, we observed a small amount of ChR2 expression in the most dorsal portion of striatum. Data from this animal was included, as all recorded cells were distant from the area of labeling, no intrinsic light responses were observed using 500 ms light pulses, and all GABAergic transmission was blocked using picrotoxin.

Histology—For histological characterization of striosome labeling in *hs599^{CreER}* mice, animals were deeply anesthetized with ketamine-xylazine (100-200 mg, IP) and transcardially perfused with 4% paraformaldehyde in PBS. Following perfusion, brains were dissected, post-fixed for 3- 12 hr, and stored in 30% sucrose at 4°C. Embryonic brains were embedded in OCT (Tissue TEK) and sectioned onto slides using a cryostat at 20uM thickness. For immunostaining, embryonic tissue was washed 3 times in PBS with 0.2% Triton X-100 and blocked with with 10% normal goat serum, 0.2% gelatin and 2% non-fat milk in PBS with 0.2% Triton X-100. Postnatal brains were sliced into 35 μm coronal sections using a freezing microtome and kept in PBS. For staining of calbindin, NPY, and PV, sections were blocked in 3% normal donkey serum (NDS) and permeabilized using 0.1% Triton X-100 for 2 hr on a shaker at 4°C. Primary antibody in 3% NDS was then added and sections incubated overnight at 4°C. Following 5 washes (10 min) with PBS, sections were incubated in 3% NDS with appropriate secondary antibody. Lastly, sections were washed 5 times with PBS and mounted in Vectashield Mounting Medium on glass slides for imaging. Immunohistochemistry for ChAT and MOR was performed with minor variations. Blocking serum for ChAT and MOR stains contained 5% NDS with 1.0% or 0.3% Triton-X, respectively. Additionally, primary antibody for MOR was incubated for 48 hr and washes were done using PBS with 0.3% Triton-X.

Primary and secondary antibodies used included: Rabbit anti-Calbindin (Swant, 1:2000), Rabbit anti-PV (Swant, 1:2000), Rabbit anti-NPY (Cell Signaling Technologies, 1:1000), Goat-anti ChAT (Millipore, 1:500), Mouse anti-NeuN (Millipore, 1:1000), Chicken anti-GFP (Aves, 1:500), Chicken anti-GFP (Abcam 1:500), Rabbit anti-RFP (Living Colors 1:1000), Rabbit anti-Ki67 (Abcam 1:300), Rabbit anti-PH3 (Millipore 1:300), Rabbit anti-Nkx2.1 (Santa Cruz Biotechnology 1:500), Rabbit anti-MOR (Immunostar, 1:2000), Rabbit anti-TH (Pel-Freez, 1:1000), Alexa Fluor 568 donkey anti-rabbit (Life Technologies, 1:500), Alexa Fluor 647 donkey anti-mouse (Jackson ImmunoResearch, 1:500), Alexa Fluor 488 donkey-anti rabbit (Jackson ImmunoResearch, 1:500), Alexa Fluor 647 donkey anti-rabbit (Jackson ImmunoResearch, 1:300), Alexa Fluor 488 goat anti-chicken (Molecular Probes 1:300) and Alexa Fluor goat anti-rabbit Cy3 (Molecular Probes 1:300).

A Nikon 6D conventional wide-field microscope was used to take stitched multi-channel fluorescence images at 4-10x when imaging whole brain sections. To colocalize tdTomato expression with other neuronal markers, multi-channel Z stacks were taken at 40x using a Nikon Spinning Disk confocal microscope. Exposure times and laser intensity were matched between all images of the same type.

Slice Electrophysiology—Mice were deeply anesthetized with ketamine-xylazine (100-200 mg, IP) and perfused with a carbogenated, ice-cold glycerol-based artificial

cereberospinal fluid (ACSF) solution containing (in mM): 250 glycerol, 2.5 KCl, 1.2 NaH$_2$PO$_4$, 10 HEPES, 21 NaHCO$_3$, 5 D-glucose, 2 MgCl$_2$, 2 CaCl$_2$. Following decapitation, brains were dissected, mounted on a chuck, and submerged in ice-cold glycerol solution. A vibrating microtome (Leica) was used to cut sequential 275 μm coronal slices containing either the striatum or the midbrain, which were immediately transferred to warm (34°C), carbogenated ACSF containing (in mM): 125 NaCl, 26 NaHCO$_3$, 2.5 KCl, 1.25 NaH$_2$PO$_4$, 12.5 D-glucose, 1 MgCl$_2$, 2 CaCl$_2$. Slices were incubated for 30-60 min, then kept at room temperature (~23°C) until use.

During all recordings, slices were superfused with carbogenated ACSF at 31-33°C. Differential interference contrast (DIC) optics on an Olympus BX 51 WIF microscope were used to target MSNs and midbrain neurons, which were patched in a whole-cell configuration using borosilicate glass electrodes (2-5 MΩ). To record excitatory synaptic currents from PL and M1 onto MSNs, we used a cesium methanesulfonate-based internal containing (in mM): 120 CsMeSO$_3$, 15 CsCl, 8 NaCl, 0.5 EGTA, 10 HEPES, pH = 7.3. Striosome and matrix MSNs within neighboring fields of view (~200 μm) were patched serially in a randomized order. Excitatory currents were optically evoked using 2 ms pulses of 473 nm light ranging in power from 0.5-10 mW and delivered by a TTL-controlled LED (Olympus) passed through a GFP filter (Chroma). Differences in intrinsic excitability between MSNs were measured using a potassium methanesulfonate-based internal containing (in mM): 130 KMeSO3,10 NaCl, 2 MgCl2, 0.16 CaCl2, 0.5 EGTA, 10 HEPES, pH = 7.3. To control for age-related changes in intrinsic excitability (Lieberman et al., 2018), animals used for these experiments were all between 90-160 days old. Picrotoxin (50 μM, Sigma Aldrich) was included in the ACSF for all intrastriatal experiments to block GABA$_A$-mediated inhibition.

To record inhibitory synaptic currents in midbrain neurons, we used a cesium methanesulfonate-based internal with high chloride, which contained (in mM): 120 CsCl, 15 CsMESO3, 8 NaCl, 0.5 EGTA, 10 HEPES, pH = 7.3. Inhibitory synaptic currents were evoked as described above. During a subset of whole-cell current clamp recordings, we examined if activation of striosome terminals was sufficient to inhibit spontaneous firing during cell-attached recordings. For these experiments, a potassium-based internal (described above) was used and 473 nm light delivered in 2 ms pulses at 20 Hz. Input resistance and holding current were measured continuously as proxies of recording stability.

All whole-cell recordings were conducted using a MultiClamp 700B amplifier (Molecular Devices) and digitized using an ITC-18 A/D board (HEKA). Igor Pro 6.0 software (Wavemetrics) and custom acquisition routines (mafPC, courtesy of M.A. Xu-Friedman). Both voltage clamp and current-clamp recordings were filtered at 5 kHz and digitized at 10 kHz.

Post hoc Identification of Recorded Neurons—Biocytin (Sigma Aldrich) was included in internal recording solutions (5 mg/mL) for experiments comparing intrinsic excitability of MSNs and synaptic input onto SNc dopamine neurons. In the first experiment, tdTomato fluorescence in the emission range of GFP confounded online identification of direct and indirect pathway neurons within striosomes in some cases, necessitating post hoc

confirmation. Three steps were taken to address this issue. First, we showed that 90.2% of tdTomato[+] MSNs belonged to the direct pathway, as described above (Figure 2K). Second, we used biocytin-fill, far-red staining for GFP, and confocal microscopy to identify recorded MSNs as direct or indirect pathway post hoc. Of all the striosome MSNs recovered, 100% (9/9) were identified as direct pathway, supporting the hypothesis recorded striosome MSNs were predominantly from the direct pathway. Finally, we compared the intrinsic excitability of identified direct pathway striosome MSNs to that of all recorded striosome MSNs and found no difference (Figure S3G). Therefore, data for striosome MSNs appeared representative of direct pathway MSNs.

For recording synaptic input to SNc dopamine neurons, biocytin was used to confirm midbrain neurons with compatible physiology as being Tyrosine-hydroxylase (TH)-expressing SNc dopamine neurons. Recorded neurons were filled for a minimum of 15 minutes before carefully detaching the recording pipette. Slices were then fixed with 4% PFA for 3-12 hr at 4°C and transferred to 30% sucrose in PBS. A sliding microtome was used to cut 55 μm subsections, which were stored in PBS until use. To identify D2-GFP in tdTomato+ cells, sections were stained with chicken anti-GFP (Aves, 1:500) and Alexa Fluor 647 Donkey anti-chicken secondary antibody (1:500), as described for NPY, PV, and calbindin stains, with Triton X-100 replaced by 0.3% Tween20 (Chem-impex Inernational Inc.). Rabbit anti-TH (1:1000, Pel Freez) and Alexa Fluor 568 Donkey anti-rabbit secondary antibody (1:500) were used to identify dopamine neurons. Alexa Fluor 350 streptavidin (3:500) was included with the secondary antibody to visualize biocytin-filled neurons. Biocytin-filled cells were located using a Nikon 6D conventional wide-field microscope at 4-10x and colocalization of fluorophores imaged using a Nikon Spinning Disk confocal microscope at 40x.

In addition to identifying dopamine neurons by post hoc staining for TH, a subset of SNc dopamine neurons were identified based on cell-attached waveforms, using criteria similar to that previously described (Chieng et al., 2011). Custom code in MATLAB was used to extract on-cell spikes based on current thresholds, which were manually determined for individual neurons. All waveforms were then manually confirmed to prevent contamination from potential artifacts. Following normalization of the peak-to-trough amplitude, normalized waveforms were averaged across each recorded neuron and the time from the peak to trough calculated. A threshold of 1 ms for peak-trough duration was selected for positive identification of dopamine neurons, as this effectively segregated biocytin-confirmed SNc dopamine neurons from neighboring GABAergic neurons in the SNr.

QUANTIFICATION AND STATISTICAL ANALYSIS

Statistics—All data are presented as the mean ± SEM, with N referring to the number of animals and n to the number of cells.

Histology and Cell Counting—Specificity and penetrance of striosome labeling in hs599[CreER];Ai14 mice was determined using coronal sections from three points along the AP-axis (+0.5, +1.0, and +1.5 mm relative to Bregma) from each animal. Striosomes and neighboring matrix regions in the dorsal half of the striatum were identified by MOR

expression using a spinning disk confocal microscope, with the experimenter imaging blinded to tdTomato[+] labeling pattern. After imaging tdTomato expression, the number of tdTomato^{+} cells were quantified manually with FIJI/ImageJ software by a rater blinded to compartmental origin. Density (Ai14^{+} cells/mm) in striosome and matrix were used as a measure of penetrance and specificity, respectively. For both measures, cell bodies within the subcallosal strip were excluded for analysis, though notably this region showed consistent MOR and tdTomato labeling across animals.

To quantify colocalization of tdTomato expression with interneuron markers (ChAT, PV, or NPY) or a marker of indirect pathway MSNs (D2-GFP), striosomes from three striatal sections along the AP-axis (+0.5, +1.0, and +1.5 relative to Bregma) were imaged in their entirety, and the number of GFP[+] and tdTomato[+] nuclei counted manually. The proportion of indirect pathway MSNs in histologically defined striosomes and matrix was quantified in D2-GFP mice using coronal striatal sections from five APs (+1.0, +0.5, 0, −0.5, and −1.0 relative to Bregma). Striosome and matrix were identified by MOR expression, and the proportion of NeuN^{+} cells positive for GFP quantified manually. The Mouse Brain Atlas in Stereotaxic Coordinates (hard copy, 4th edition, by George Paxinos and Keither B.J Franklin) was consulted for anatomical reference.

Slice Electrophysiology—To characterize intrinsic excitability, custom code in Igor Pro (Wavemetrics) was used to extract the instantaneous firing rate for each current step, rheobase, maximum firing rate, and resting membrane potential. Input resistance was manually calculated using Ohm's law ($V = I*R$) and the current transient induced by a −5 mV step from −70 mV holding in voltage clamp. For all measures, significance was determined using a Kruskal-Wallis test with a Bonferroni correction applied to control for multiple comparisons. A Dunn's post hoc test was applied to test for significance between individual groups. The positive and negative predictive values of various rheobase thresholds to identify striosome from matrix MSNs were calculated using the following equations: [positive predictive value = true positives / (true positives + false positives)], [negative predictive value = true negatives / (true negatives + false negatives)].

Average amplitudes of oEPSCs and oIPSCs were quantified manually in Igor. A Wilcoxon sign-rank test was used to compare oEPSC amplitude from M1 or PL onto striosome and matrix MSNs. For comparison of oIPSC amplitude onto midbrain neurons, we used a Wilcoxon rank-sum test. In all experiments involving optical stimulation, data was drawn from stimulations at ~3.5 mW light power.

To determine if the observed output of striosome and direct pathway matrix MSNs to SNr and SNc neurons differed statistically, 50% of oIPSC amplitudes from SNr and SNc neurons were randomly sampled with replacement 10,000 times for each genotype using custom MATLAB code (Mathworks). For each trial, the ratio of output (SNr:SNc) was calculated using the average oIPSC amplitude sampled from each cell type. Ratios were binned in units of 1 and the probability density distributions obtained by dividing the total number of counts in each bin by the total number of trials. A Kolmogorov–Smirnov test was used to test for differences between the probability distribution obtained from *hs599^{CrsER}*;Ai32 and D1-Cre;Ai32 mice.

DATA AND CODE AVAILABILITY

Any data or code supporting the current study are available from the Lead Contact upon request.

Supplementary Material

Refer to Web version on PubMed Central for supplementary material.

ACKNOWLEDGMENTS

REFERENCES

Banghart MR, Neufeld SQ, Wong NC, and Sabatini BL (2015). Enkephalin disinhibits mu opioid receptor rich striatal patches via delta opioid receptors. Neuron 88, 1227–1239. [PubMed: 26671460]

Bloem B, Huda R, Sur M, and Graybiel AM (2017). Two-photon imaging in mice shows striosomes and matrix have overlapping but differential reinforcement-related responses. eLife 6, e32353. [PubMed: 29251596]

Brown J, Bullock D, and Grossberg S (1999). How the basal ganglia use parallel excitatory and inhibitory learning pathways to selectively respond to unexpected rewarding cues. J. Neurosci. 19, 10502–10511. [PubMed: 10575046]

Chieng B, Azriel Y, Mohammadi S, and Christie MJ (2011). Distinct cellular properties of identified dopaminergic and GABAergic neurons in the mouse ventral tegmental area. J. Physiol. 589, 3775–3787. [PubMed: 21646409]

Crittenden JR, Lacey CJ, Weng F-J, Garrison CE, Gibson DJ, Lin Y, and Graybiel AM (2017). Striatal cholinergic interneurons modulate spiketiming in striosomes and matrix by an amphetamine-sensitive mechanism. Front. Neuroanat. 11, 20. [PubMed: 28377698]

Cui G, Jun SB, Jin X, Pham MD, Vogel SS, Lovinger DM, and Costa RM (2013). Concurrent activation ofstriatal direct and indirect pathways during action initiation. Nature 494, 238–242. [PubMed: 23354054]

Davis MI, and Puhl HL 3rd. (2011). Nr4a1-eGFP is a marker of striosome-matrix architecture, development and activity in the extended striatum. PLoS ONE 6, e16619. [PubMed: 21305052]

Dodson PD, Larvin JT, Duffell JM, Garas FN, Doig NM, Kessaris N, Duguid IC, Bogacz R, Butt SJB, and Magill PJ (2015). Distinct developmental origins manifest in the specialized encoding of movement by adult neurons of the external globus pallidus. Neuron 86, 501–513. [PubMed: 25843402]

Eblen F, and Graybiel AM (1995). Highly restricted origin of prefrontal cortical inputs to striosomes in the macaque monkey. J. Neurosci. 15, 5999–6013. [PubMed: 7666184]

Flandin P, Kimura S, and Rubenstein JLR (2010). The progenitor zone of the ventral medial ganglionic eminence requires Nkx2-1 to generate most of the globus pallidus but few neocortical interneurons. J. Neurosci. 30, 2812–2823. [PubMed: 20181579]

Friedman A, Homma D, Gibb LG, Amemori K, Rubin SJ, Hood AS, Riad MH, and Graybiel AM (2015). A corticostriatal path targeting striosomes controls decision-making under conflict. Cell 161, 1320–1333. [PubMed: 26027737]

Friedman A, Homma D, Bloem B, Gibb LG, Amemori KI, Hu D, Delcasso S, Truong TF, Yang J, Hood AS, et al. (2017). Chronic stress alters striosome-circuit dynamics, leading to aberrant decision-making. Cell 171, 1191–1205.e28. [PubMed: 29149606]

Fujiyama F, Sohn J, Nakano T, Furuta T, Nakamura KC, Matsuda W, and Kaneko T (2011). Exclusive and common targets of neostriatofugal projections of rat striosome neurons: a single neuron-tracing study using a viral vector. Eur. J. Neurosci. 33, 668–677. [PubMed: 21314848]

Gerfen CR (1985). The neostriatal mosaic. I. Compartmental organization of projections from the striatum to the substantia nigra in the rat. J. Comp. Neurol. 236, 454–476. [PubMed: 2414339]

Gerfen CR, Baimbridge KG, and Miller JJ (1985). The neostriatal mosaic: compartmental distribution of calcium-binding protein and parvalbumin in the basal ganglia of the rat and monkey. Proc. Natl. Acad. Sci. USA 82, 8780–8784. [PubMed: 3909155]

Gerfen CR, Paletzki R, and Heintz N (2013). GENSAT BAC cre-recombinase driver lines to study the functional organization of cerebral cortical and basal ganglia circuits. Neuron 80, 1368–1383. [PubMed: 24360541]

Gertler TS, Chan CS, and Surmeier DJ (2008). Dichotomous anatomical properties of adult striatal medium spiny neurons. J. Neurosci. 28, 10814–10824. [PubMed: 18945889]

Gong S, Zheng C, Doughty ML, Losos K, Didkovsky N, Schambra UB, Nowak NJ, Joyner A, Leblanc G, Hatten ME, and Heintz N (2003). A gene expression atlas of the central nervous system based on bacterial artificial chromosomes. Nature 425, 917–925. [PubMed: 14586460]

Hernández VM, Hegeman DJ, Cui Q, Kelver DA, Fiske MP, Glajch KE, Pitt JE, Huang TY, Justice NJ, and Chan CS (2015). Parvalbumin+ neurons and Npas1+ neurons are distinct neuron classes in the mouse external globus pallidus. J. Neurosci. 35, 11830–11847. [PubMed: 26311767]

Jiménez-Castellanos J, and Graybiel AM (1989). Compartmental origins of striatal efferent projections in the cat. Neuroscience 32, 297–321. [PubMed: 2479881]

Kawaguchi Y, Wilson CJ, and Emson PC (1989). Intracellular recording of identified neostriatal patch and matrixspiny cells in a slice preparation preserving cortical inputs. J. Neurophysiol. 62, 1052–1068. [PubMed: 2585039]

Kelly SM, Raudales R, He M, Lee JH, Kim Y, Gibb LG, Wu P, Matho K, Osten P, Graybiel AM, and Huang ZJ (2018). Radial glial lineage progression and differential intermediate progenitor amplification underlie striatal compartments and circuit organization. Neuron 99, 345–361.e4. [PubMed: 30017396]

Kincaid AE, and Wilson CJ (1996). Corticostriatal innervation of the patch and matrix in the rat neostriatum. J. Comp. Neurol. 374, 578–592. [PubMed: 8910736]

Kravitz AV, and Kreitzer AC (2012). Striatal mechanisms underlying movement, reinforcement, and punishment. Physiology 27, 167–177. [PubMed: 22689792]

Lévesque M, and Parent A (1998). Axonal arborization of corticostriatal and corticothalamic fibers arising from prelimbic cortex in the rat. Cereb. Cortex 8, 602–613. [PubMed: 9823481]

Lieberman OJ, McGuirt AF, Mosharov EV, Pigulevskiy I, Hobson BD, Choi S, Frier MD, Santini E, Borgkvist A, and Sulzer D (2018). Dopamine triggers the maturation of striatal spiny projection neuron excitability during a critical period. Neuron 99, 540–554.e4. [PubMed: 30057204]

Lopez-Huerta VG, Nakano Y, Bausenwein J, Jaidar O, Lazarus M, Cherassse Y, Garcia-Munoz M, and Arbuthnott G (2016). The neostriatum: two entities, one structure? Brain Struct. Funct 221, 1737–1749. [PubMed: 25652680]

Madisen L, Zwingman TA, Sunkin SM, Oh SW, Zariwala HA, Gu H, Ng LL, Palmiter RD, Hawrylycz MJ, Jones AR, et al. (2010). A robust and high-throughput Cre reporting and characterization system for the whole mouse brain. Nat. Neurosci. 13, 133–140. [PubMed: 20023653]

Madisen L, Mao T, Koch H, Zhuo JM, Berenyi A, Fujisawa S, Hsu Y-WA, Garcia AJ 3rd, Gu X, Zanella S, et al. (2012). A toolbox of Credependent optogenetic transgenic mice for light-induced activation and silencing. Nat. Neurosci. 15, 793–802. [PubMed: 22446880]

Mason HA, Rakowiecki SM, Raftopoulou M, Nery S, Huang Y, Gridley T, and Fishell G (2005). Notch signaling coordinates the patterning of striatal compartments. Development 132, 4247–4258. [PubMed: 16120638]

Miyamoto Y, Katayama S, Shigematsu N, Nishi A, and Fukuda T (2018). Striosome-based map of the mouse striatum that is conformable to both cortical afferent topography and uneven distributions of dopamine D1 and D2 receptor-expressing cells. Brain Struct. Funct. 223, 4275–4291. [PubMed: 30203304]

Nóbrega-Pereira S, Gelman D, Bartolini G, Pla R, Pierani A, and Marín O (2010). Origin and molecular specification of globus pallidus neurons. J. Neurosci. 30, 2824–2834. [PubMed: 20181580]

Pert CB, Kuhar MJ, and Snyder SH (1976). Opiate receptor: autoradiographic localization in rat brain. Proc. Natl. Acad. Sci. USA 73, 3729–3733. [PubMed: 185626]

Planert H, Berger TK, and Silberg G (2013). Membrane properties of striatal direct and indirect pathway neurons in mouse and rat slices and their modulation by dopamine. PLoS ONE 8, e57054. [PubMed: 23469183]

Ragsdale CW Jr., and Graybiel AM (1988). Fibers from the basolateral nucleus of the amygdala selectively innervate striosomes in the caudate nucleus of the cat. J. Comp. Neurol. 269, 506–522. [PubMed: 2453535]

Sadikot AF, Parent A, Smith Y, and Bolam JP (1992). Efferent connections of the centromedian and parafascicular thalamic nuclei in the squirrel monkey: a light and electron microscopic study of the thalamostriatal projection in relation to striatal heterogeneity. J. Comp. Neurol. 320, 228–242. [PubMed: 1619051]

Silberberg SN, Taher L, Lindtner S, Sandberg M, Nord AS, Vogt D, Mckinsey GL, Hoch R, Pattabiraman K, Zhang D, et al. (2016). Subpallial enhancer transgenic lines: a data and tool resource to study transcriptional regulation of GABAergic cell fate. Neuron 92, 59–74. [PubMed: 27710791]

Smith JB, Klug JR, Ross DL, Howard CD, Hollon NG, Ko VI, Hoffman H, Callaway EM, Gerfen CR, and Jin X (2016). Genetic-based dissection unveils the inputs and outputs of striatal patch and matrix compartments. Neuron 91, 1069–1084. [PubMed: 27568516]

van der Kooy D, and Fishell G (1987). Neuronal birthdate underlies the development of striatal compartments. Brain Res. 401, 155–161. [PubMed: 3028569]

Visel A, Taher L, Girgis H, May D, Golonzhka O, Hoch RV, McKinsey GL, Pattabiraman K, Silberberg SN, Blow MJ, et al. (2013). A high-resolution enhancer atlas of the developing telencephalon. Cell 152, 895–908. [PubMed: 23375746]

Watabe-Uchida M, Zhu L, Ogawa SK, Vamanrao A, and Uchida N (2012). Whole-brain mapping of direct inputs to midbrain dopamine neurons. Neuron 74, 858–873. [PubMed: 22681690]

Yang H, de Jong JW, Tak Y, Peck J, Bateup HS, and Lammel S (2018). Nucleus accumbens subnuclei regulate motivated behavior via direct inhibition and disinhibition of VTA dopamine subpopulations. Neuron 97, 434–449.e4. [PubMed: 29307710]

Yoshizawa T, Ito M, and Doya K (2018). Reward-predictive neural activities in striatal striosome compartments. eNeuro 5, 5.

Highlights

- *hs599*^{CreER} mice enable labeling of direct pathway striosome MSNs

- Striosome and matrix MSNs receive biased input from prelimbic and primary motor cortex

- Striosome MSNs show higher intrinsic excitability than matrix MSNs

- Striosome MSNs are the predominant striatal population innervating SNc dopamine neurons
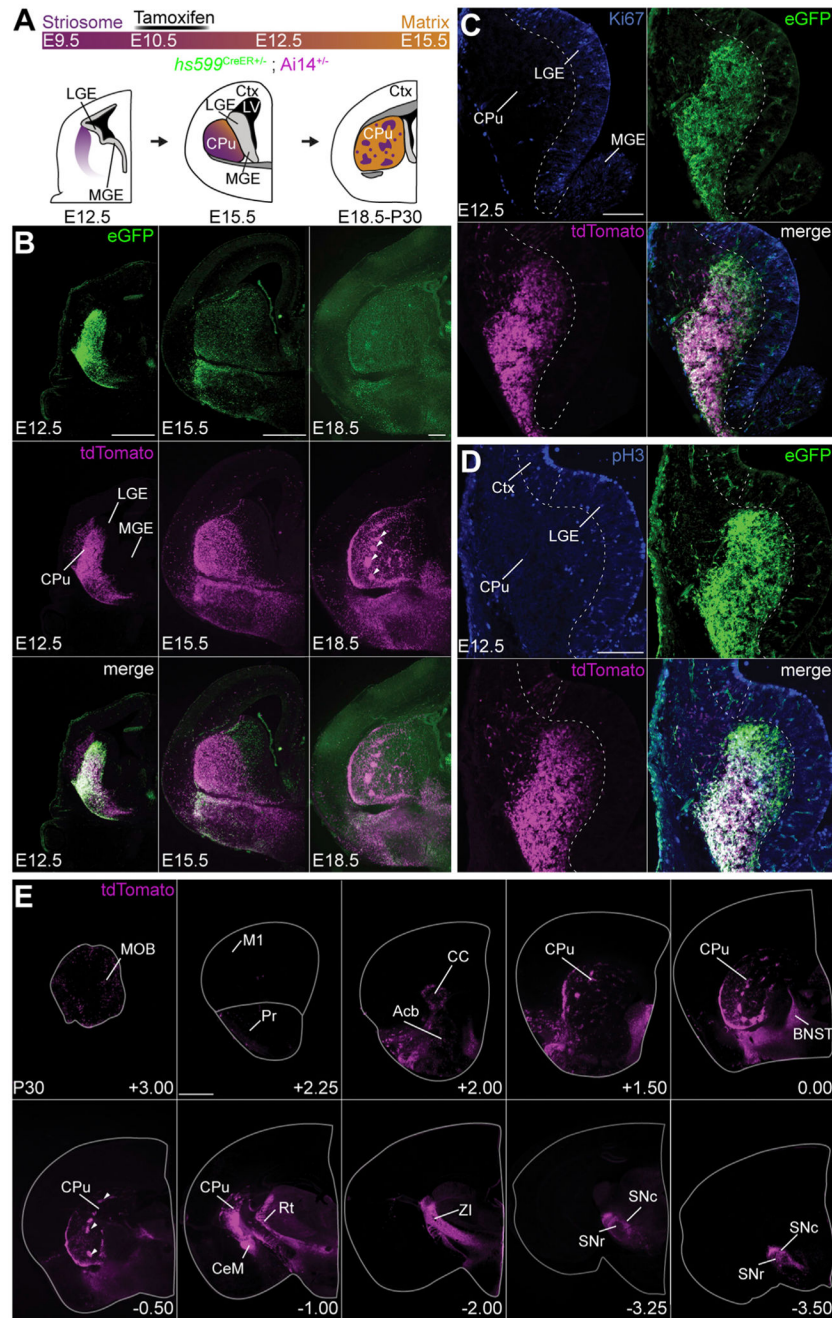
Figure 1. Targeting of Early-Born Striatal Neurons Using _hs599^{CreER}_ Mice

(A) Schematic of striosome (purple) and matrix (orange) development and strategy for using tamoxifen to capture early born striatal neurons. CPu, caudoputamen (striatum); Ctx, cortex; LGE, lateral ganglionic eminence; LV, lateral ventricle; MGE, medial ganglionic eminence).

(B) tdTomato$^+$ (magenta) and CreER-eGFP$^+$ (green) cells at E12.5 (left), E15.5 (middle), and E18.5 (right) following E10.5 tamoxifen administration. Arrows indicate potential striosomes.

(C and D) Overlap of tdTomato$^+$ and CreER-EGFP$^+$ cells with progenitor cells marked by (C) Ki67 (blue) or (D) phospho-histone H3 (pH3, blue).

(E) Sample coronal sections illustrating tdTomato-labeled structures in the adult brain (P30) following tamoxifen administration at E10.5. The anteroposterior distance from bregma (in mm) is noted in the lower right corner of each panel.

MOB, main olfactory bulb; M1, primary motorcortex; Pr, piriform cortex; CC, corpus callosum; acb, nucleus accumbens; str, striatum; BNST, bed nucleus of the stria terminalis; Rt, reticular thalamus, CeM, central amygdala; ZI, zona incerta; SNr, substantia nigra pars reticulata; SNc, substantia nigra pars compacta. Scale bars represent 0.5 μm (B and E) and 50 μm (C and D). See also Figures S1 and S2.
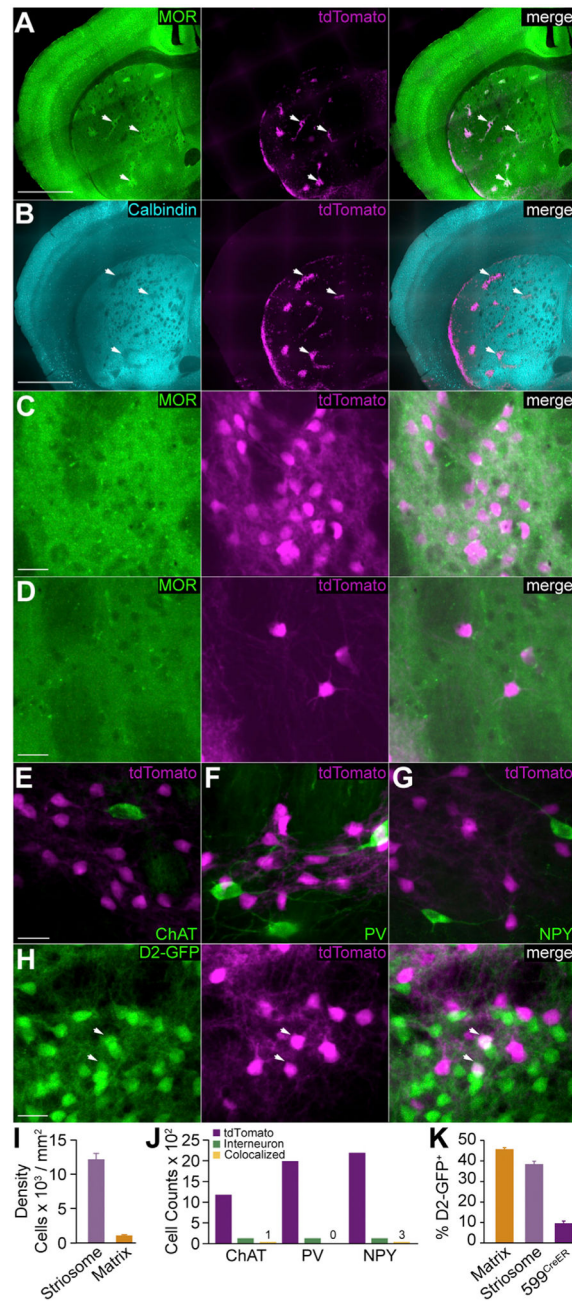
Figure 2. _hs599^CreER_ Mice Enable Targeting of Striosome MSNs

(A and B) Overlap of tdTomato^{+} cells (magenta) in striosomes (arrows) identified by (A) increased μ-opioid receptor (MOR; green) or (B) decreased calbindin (blue) staining.

(C and D) Example of high-magnification image used to quantify the density tdTomato^{+} cells in (C) striosome and (D) matrix compartments as identified by MOR staining.

(E–G) Overlap of tdTomato^{+} cells with interneurons (green), marked by staining for (E) choline acetyltransferase (ChAT), (F) parvalbumin (PV), and (G) neuropeptide Y (NPY).

(H)Example of overlap between tdTomato[+] and D2-GFP^{+} cells.

(I)Quantification of tdTomato[+] cell density in striosome and matrix.

(J)Cell counts of tdTomato$^+$ cells, interneurons, and double-labeled cells for ChAT, PV, and NPY.

(K)Percentage of matrix, striosome, and tdTomato$^+$ cells that are D2-GFP$^+$.

Scale bars represent 1.0 mm (A and B) and 20 μm (C–H). Data are displayed as mean ± SEM.
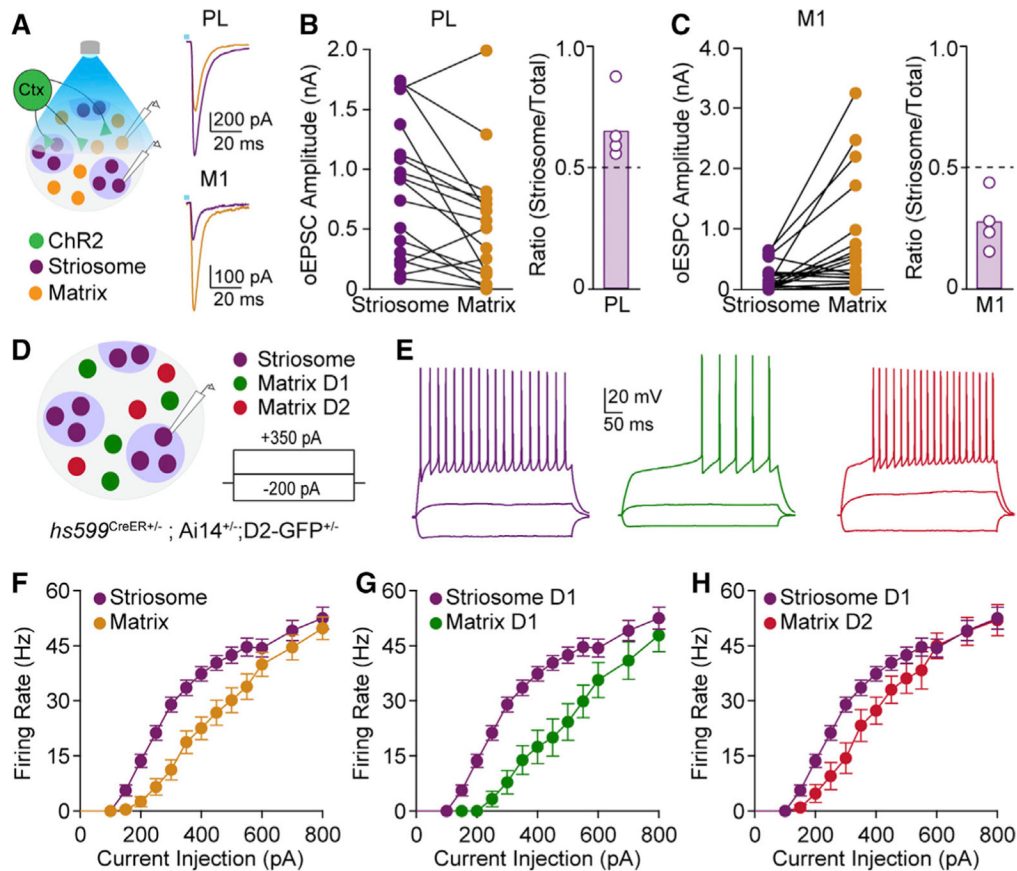
Figure 3. Cortical Innervation and Intrinsic Excitability Differs between Striosome and Matrix MSNs

(A) Schematic of recording configuration (left) and examples of optically evoked excitatory post-synaptic currents (oEPSCs) from prelimbic (PL, top right) and primary motor (M1, bottom right) cortex in striosome (purple) and matrix neurons (orange).

(B) Left: amplitudes of oEPSCs from PL cortex in sequential pairs of striosome and matrix neurons. Right: bias of PL for striosome based on oEPSC amplitudes. Bar represents the average for all recorded pairs, while individual points represent the average calculated for individual animals. A value of 1 represents input exclusively to striosome neurons, while a value of 0 represents input exclusively to matrix neurons.

(C) Left: amplitudes of oEPSCs from M1 cortex in sequential pairs of striosome and matrix neurons. Right: bias of M1 input for matrix calculated as in (B).

(D) Schematic of excitability recording configuration.

(E) Responses of a direct pathway striosome (purple), direct pathway matrix (green), and indirect pathway matrix (red) to three example current injections.

(F–H) Current-frequency plot for (F) all striosome and matrix MSNs, (G) direct pathway striosome and matrix MSNs, and (H) direct pathway striosome and indirect pathway matrix MSNs.

Data are displayed as mean ± SEM. See also Figure S3.
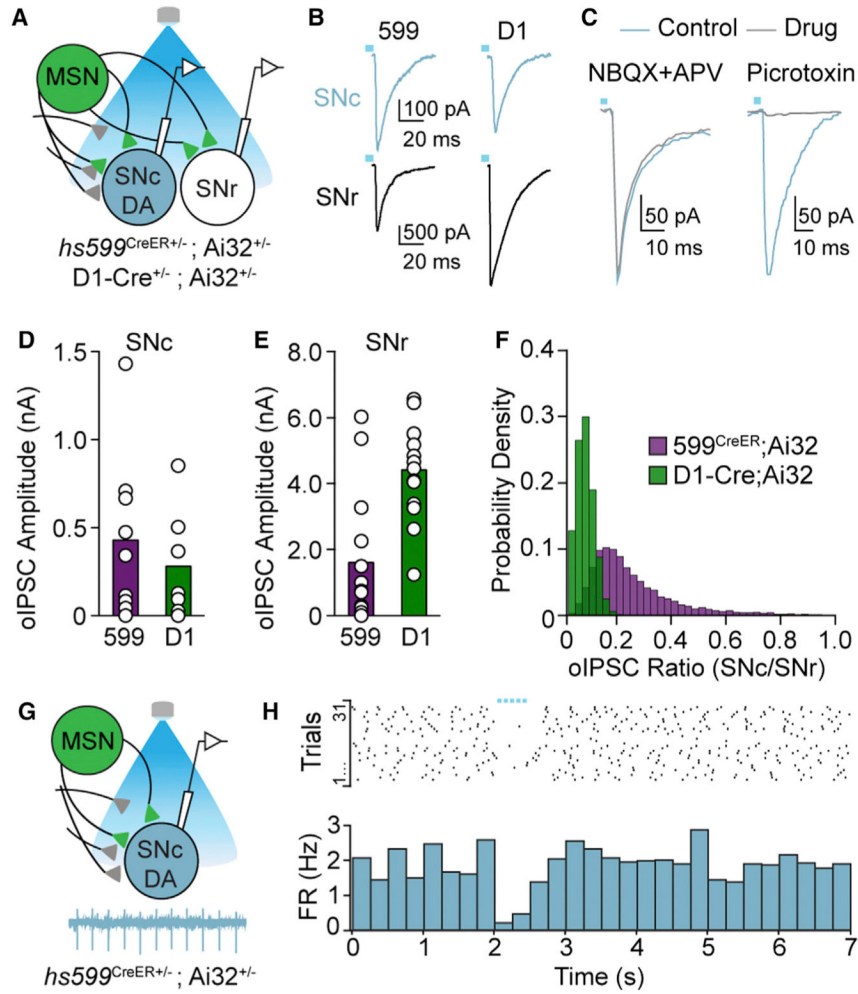
Figure 4. Striosome Output to Midbrain Neurons Is Distinct from Direct Pathway MSNs

(A) Schematic of recording configuration.

(B) Example optically evoked inhibitory currents (oIPSCs) in SNc dopamine (blue) and SNr (black) neurons from hs599[CreER];Ai32 (left) and D1-Cre;Ai32 (right) mice.

(C) Effect of NBQX and APV or picrotoxin on oIPSCs in a SNc dopamine neuron from a *hs599[CreER]*;Ai32 mouse.

(D) oIPSC amplitudes in SNr dopamine neurons for striosome and direct pathway terminal stimulation.

(E) oIPSC amplitudes in SNc neurons for striosome and direct pathway terminal stimulation.

(F) Probability density plot of oIPSC amplitude ratios (SNc:SNr) obtained by bootstrapping data from *hs599[CreER]* (green) and D1-Cre (purple) mice.

(G) Configuration for cell-attached recording of SNc dopamine neurons with example trace.

(H) Top: raster of spontaneous SNc DA neuron firing (31 trials across 7 cells) with suppression by striosome terminal stimulation (blue bars). Bottom: firing rates over time (500-ms bins) for all dopamine neurons.

Data are displayed as the mean. See also Figure S4.

KEY RESOURCES TABLE

REAGENT or RESOURCE	SOURCE	IDENTIFIER
Antibodies		
Rabbit anti-TH	Pel-Freez Biologicals	Cat# P40101-150; RRID: AB_2617184
Goat anti-ChAT	Millipore	Cat# AB144P; RRID: AB_2079751
Rabbit anti-NPY	Cell Signaling Technology	Cat# 11976; RRID: AB_2716286. Lot#1
Rabbit anti-PV	Swant	Cat# PV27; RRID: AB_2631173
Mouse anti-NeuN	Millipore	Cat# MAB377; RRID: AB_2298772
Chicken anti-GFP	Aves	Cat# GFP-1020; RRID: AB_2307313
Chicken anti-GFP	Abcam	Cat# ab13970; RRID: AB_300798
Rabbit anti-RFP	Living Colors	Cat# 632496; RRID: AB_10013483
Rabbit anti-Ki67	Abcam	Cat# ab16667; RRID: AB_302459
Rabbit anti-PH3	Millipore	Cat# 06_570; RRID: AB_310177
Rabbit anti-Nkx2.1	Santa Cruz Biotechnology	Cat# sc-13040; RRID: AB_793532
Rabbit anti-MOR	Immunostar	Cat# 24216; RRID: AB_572251
Rabbit anti-Calbindin D-28k	Swant	Cat# CB-38a; RRID:AB_10000340
Alexa Fluor 350- Streptavadin	Invitrogen	Cat# S11249; Lot #1856878
Alexa Fluor488- Donkey anti-Rabbit IgG	Jackson ImmunoResarch	Cat# 711-546-152; RRID: AB_2340619
Alexa Fluor488- Donkey anti-Goat IgG	Jackson ImmunoResarch	Cat# 705-545-147; RRID: AB_2336933
Alexa Fluor- Donkey anti-Goat IgG – Cy3	Jackson ImmunoResarch	Cat# 705-165-147; RRID: AB_2307351
Alexa Fluor488- Donkey anti-Chicken IgY (IgG)	Jackson ImmunoResarch	Cat# 703-545-155; RRID: AB2340375
Alexa Fluor568- Donkey anti-Rabbit IgG	Invitrogen	Cat# A10042; RRID: AB_2534017
Alexa Fluor647- Donkey anti-Rabbit IgG	Jackson ImmunoResarch	Cat# 711-606-152; RRID: AB_2340625
Alexa Fluor647- Donkey anti-Chicken IgY (IgG)	Jackson ImmunoResarch	Cat# 703-606-155; RRID: AB_2340380
Bacterial and Virus Strains		
rAAV5-hSyn-hChR2(H134R)-EYFP	UNC Vector Core	Lot AV4319I
Chemicals, Peptides, and Recombinant Proteins		
Picrotoxin	Sigma-Aldrich	P1675
Lidocaine N-ethyl chloride	Sigma-Aldrich	L1663
Potassium methanesulfonate	Sigma-Aldrich	83000
Cesium methanesulfonate	Sigma-Aldrich	C1426
Cesium Chloride	Sigma-Aldrich	C3139
Guanosine 5′-triphosphate sodium salt hydrate	Sigma-Aldrich	A9187
Adenosine 5′-triphosphate magnesium salt	Sigma-Aldrich	D3900
CNQX	Tocris	1045
D-APV	Tocris	0106
Corn Oil	Fisher Scientific	S25271

REAGENT or RESOURCE	SOURCE	IDENTIFIER
Tamoxifen	Sigma-Aldrich	T5648
Proteinase K	Promega	V3021
TaKaRa LA Taq	TaKaRa	RR002M
IGEPAL CA-630	Sigma-Aldrich	I3021
Tween20	Chem-Impex International	50-493-594
Triton X-100	Sigma-Aldrich	T8787
Biocytin	Sigma-Aldrich	B4261
Vectashield Mounting Medium with DAPI	Vector Laboratories	H-1200
Tissue –Tek OCT Compund	VWR	25608-930
Experimental Models: Organisms/Strains		
Mouse: WT: Crl:CD1(ICR)	Charles River	RRID:IMSR_CRL:22
Mouse: STOCK Tg(Drd2-EGFP)S118Gsat/Mmnc *Mus musculus*	MMRRC	RRID: MMRRC_000230-UNC
Mouse: B6.Cg-Gt(ROSA)26sor$^{tm14(CAG-tdTomato)Hze}$/J	The Jackson Laboratory	RRID: IMSR_JAX:007914
Mouse: Gt(ROSA)$^{26Sortm32(CAG-COP4*H134R/EYFP)Hze}$	The Jackson Laboratory	RRID:IMSR_JAX:012569
Mouse: B6.FVB(Cg)-Tg(Drd1cre)EY217Gsat/Mmucd	MMRRC	RRID: MMRRC_034258-UCD
Mouse: STOCK Tg(hs599-cre/ERT2,-GFP)119Jlr/Mmucd	Laboratory of John Rubenstein	RRID:MMRRC_041445-UCD
Oligonucleotides		
hs599^{CreER} Forward PCR Primer: CACTACTGTTTCTAAG TGTTTCC	This paper	N/A
hs599^{CreER} Reverse PCR Primer: CAGCACAGGCTCAAAG TTGCC	This paper	N/A
Software and Algorithms		
Igor Pro	Wavemetrics	https://www.wavemetrics.com/products/igorpro/igorpro.htm; RRID: SCR_000325
Axon MultiClamp Commander Software	Axon	http://mdc.custhelp.com/app/answers/detail/a_id/18877/~/axon%E2%84%A2-multiclamp%E2%84%A2-commander-software-download-page
MATLAB R2018a	Mathworks	https://www.mathworks.com/products/matlab.html; RRID: SCR_001622
Adobe Illustrator CS6	Adobe	https://www.adobe.com/products/illustrator.html; RRID: SCR_014198
ImageJ	NIH	https://imagej.net/Welcome; RRID:SCR_003070
NIS-Elements	Nikon	https://www.microscope.healthcare.nikon.com/products/software; RRID:SCR_014329
mafPC	Xu-Friedman Lab	https://www.xufriedman.org/mafpc;
Other		
Single Channel Temperature Controller	Warner Instruments	TC-324C
MINIPULS 3 Peristaltic Pumps	Gilson	F155008
X-Cite 120LED Boost	Excelitas	010-00326R
ITC-18 16-bit Multi-Channel Data Acquisition Interface	Heka	ITC-18
MultiClamp 700B Microelectrode Amplifier	Molecular Devices	Multiclamp 700b
Headstage CV-7B	Molecular Devices	Mo-1-CV-7B
Fixed Stage Microscope	Olympus	BX51WI